Proceedings of BS2013:
13th Conference of International Building Performance Simulation Association, Chambéry, France, August 26-28

NUMERICAL INVESTIGATION OF NATURAL CONVECTION IN AN ASYMMETRICALLY HEATED INCLINED CHANNEL-CHIMNEY SYSTEMS IMPORTANCE OF THE CHOICE OF ARTIFICIAL INLET-OUTLET BOUNDARY CONDITIONS

Boris Brangeon[1,3], Patrice Joubert[2] and Alain Bastide[3]
[1]TREFLE, Université de Bordeaux 1, Bordeaux, France
[2]LaSIE, Université de la Rochelle, La Rochelle, France
[3]PIMENT, Université de la Réunion, Le Tampon, France

ABSTRACT

The present paper is concerned with the results of the numerical investigation of unsteady laminar, natural convection in an asymmetrically heated inclined open channel ($i = 0, 45, 60$ and $75°$) with walls at uniform heat flux ($q_w = 10, 50, 75$ and $100\mathrm{W}\cdot\mathrm{m}^{-2}$). Two methodological approaches have been adopted to investigate the air flow in this case: 2D and 3D DNS, and four sets of inlet-outlet velocity-pressure boundary conditions have been considered. Significant differences are observed in the flow dynamics between 2D and 3D results. The numerical results are compared with the experimental data and a good agreement is obtained when a local pressure boundary condition is applied at the inlet/outlet sections in the 3D case. A generalized correlation for the average Nusselt number is then obtained from numerical results. This correlation covers a wide range of the Rayleigh number and aspect ratio values (Ra_H varying from 5.89×10^9 to 5.89×10^{10} and $6.5 < H/b < 12.8$).

INTRODUCTION

Passive systems based on buoyant flows developing in heated vertical or inclined channels are used in many engineering applications such as solar chimneys, photovoltaic cooling systems, or devices for air conditioning and natural ventilation in buildings. Recent papers can be found in the literature for such configurations, as well from an experimental (Chami and Zoughaib, 2010; Popa et al., 2012) than for an analytical or numerical point of view (Bassiouny and Korah, 2009; Suárez et al., 2011), in continuation of numerous previous works during the last decades. (Elenbaas, 1942) pioneered the experimental investigation of natural convection of air within a vertical parallel-plate channels and identified the different types of flows regimes, according to the definition of a modified Rayleigh number. (Bar-Cohen and Rohsenow, 1984) derived a set of correlations for the Nusselt number in an asymmetrically heated channel. (Sparrow et al., 1984) highlighted on their wall the possibility of a reverse flow at the upper end of a channel heated at a constant temperature on one side. More recently, the domain of existence of reverse flow was deeply experimentally investigated by (Dupont et al., 2007) and (Samot et al., 2010) for a constant flux wall heated channel. From a numerical point of view, imposition of coherent boundary conditions at the geometrical limits of the computational domain is not obvious because velocity and pressure values are not known a priori at the inlet and outlet sections of the channel. Different strategies are then available. One is to consider extended domains at the entrance and at the exit of the channel where free stress or non rotational flow conditions can be applied. (Naylor et al., 1991) considered as an example a semi-circular extension at the entrance of the channel with a (Jeffery, 1915) and (Hamel, 1916) flow approximation at the perimeter of this domain. (Andreozzi et al., 2007) and (Campo et al., 1997) considered inlet and outlet rectangular extensions at both ends of the channel.
The problem of such extensions is that the natural convection flow that develops in the channel is very sensitive to the size of the extensions, and boundary conditions must be rejected very far form the inlet/outlet of the channel. (Suárez et al., 2011) found in that way that the computational domain including the whole channel they consider must be 200 times larger and higher than the channel itself for assuming independence of the flow and heat transfer in the channel from the external surrounding domain.

In order to focus on the flow and heat transfer in the channel, we will consider in this study a computational domain restricted to the channel geometry because increasing the size of the computational domain is expensive in terms of memory and computational time. This raises the question of defining a physically coherent set for the boundary conditions at the inlet and outlet of the channel, that enables in particular recirculation of the fluid inside the channel.

The problem is the choice of artificial inlet boundary conditions and their numerical implementation (Le Quéré, 2008). Hence, it follows that two and three dimensional natural convection in inclined channels with open boundaries has been rarely investigated using inlet-outlet boundary conditions. In order to investigate the influence of the boundary condition imposed at the ends of a heated vertical or inclined channel on the natural convection flow inside the channel, an in-house DNS numerical code has been developed. The configurations we consider are similar to those experimentally investigated by (Webb and Hill, 1989; Dupont et al., 2007) and (Samot et al., 2010). We defined different sets of pressure-velocity boundary

conditions, either for 2D and 3D computations. The experimental data available from the experiments provide relevant information for comparison with the numerical simulations in terms of heat transfer at the heated wall, mass flow rate in the channel, but also for velocity and temperature profiles.

In the first part of the paper, the numerical approach is introduced and different sets of pressure-velocity boundary conditions are discussed. Then 2D and 3D results are compared with experimental data, particularly for the existence of a reversal flow over a wide range of Rayleigh number. Finally, a generalized correlation for the average Nusselt number is proposed from the 2D numerical results, for values of the Rayleigh number varying from $Ra_H = 5.89 \times 10^9$ to 5.89×10^{10} and for aspect ratio $6.5 < H/b < 12.8$.

PROBLEM DESCRIPTION

Geometry

First, we consider a two-dimensional open channel asymmetrically heated by a constant parietal heat flux imposed on its left side (see Figure 1). The channel is made of a set of two parallel rectangular plates of dimension $H \times l$ with $H = 0.64\,\mathrm{m}$. For three-dimensional numerical investigation the depth $l = 0.304\,\mathrm{m}$ is considered.

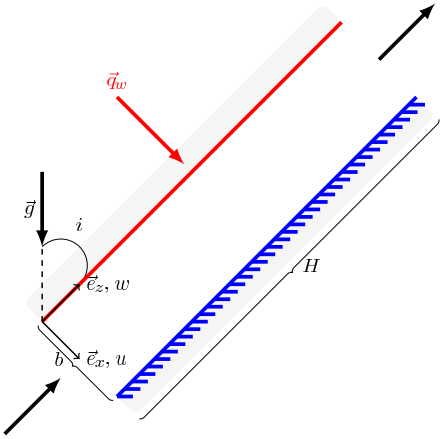

Figure 1: Computational domain. Asymmetric inclined channel heated at uniform heat flux

In the present investigation, different heat fluxes and three channel widths are studied, namely: $q_w = 10$, 50, 75 and $100\,\mathrm{W \cdot m^{-2}}$ and $b = 0.05$, 0.06 and $0.1\,\mathrm{m}$, resulting in aspect ratios (H/b) of the channel equal to 6.5; 10.67 and 12.8 respectively. Thirty cases were considered, which are summarized in Table 1.

Governing equations

Computational fluid dynamics (CFD) approach is employed to simulate the airflow and heat transfer in the inclined channel system. The continuity (1), momentum (2) and energy (3) equations for a two-dimensional laminar flow of an incompressible Newtonian fluid under the Boussinesq approximation are used. The equations in dimensionless form, using H as the reference length, $V_{ref} = \frac{\kappa}{H} Ra_H^{1/2}$ as the reference natural convection velocity, and $\Delta T = q_w b/\lambda$ as temperature difference, are:

$$\frac{\partial u_i}{\partial x_i} = 0 \tag{1}$$

$$\frac{\partial u_i}{\partial t} + \frac{\partial u_i u_j}{\partial x_j} = -\frac{\partial P}{\partial x_i} + \Pr\, Ra_H^{-1/2} \frac{\partial^2 u_i}{\partial x_j \partial x_j} + Pr\theta(\sin(i)\delta_{ix} - \cos(i)\delta_{iz}) \tag{2}$$

$$\frac{\partial \theta}{\partial t} + \frac{\partial u_j \theta}{\partial x_j} = Ra_H^{-1/2} \frac{\partial^2 \theta}{\partial x_j \partial x_j} \tag{3}$$

Ra_H is the Rayleigh number based on the height of the cavity, and Pr is the Prandtl number. Here β, ν and κ are respectively the coefficient of volumetric expansion, kinematic viscosity, and thermal diffusivity. The thermophysical air properties were all evaluated at the reference temperature $T_0 = 298\,\mathrm{K}$, and $Pr = 0.71$.

NUMERICAL APPROACH

The configuration considered in the present study is presented in Figure 1. The spatial discretization is achieved with a finite-volume method on collocated grids. Grid spacing in the x-direction is uniform and the wall-normal points are distributed using a cosine distribution (Henkes and Hoogendoorn, 1995):

$$x(i) = \frac{b}{2H}\left\{1 - \cos\left(\frac{\pi(i-1)}{N-1}\right)\right\} \tag{4}$$

Time derivatives in the momentum and the energy equations are approximated by a second-order backward differentiation scheme. An implicit formulation is employed for the diffusion terms. An explicit second-order backward Adams Bashforth extrapolation for the nonlinear terms is implemented. Finally, the spatial and time derivatives are approximate with second-order schemes. A Pressure Implicit with Splitting of Operators (PISO, (Issa, 1986)) procedure is used for the pressure-velocity coupling. A 64×512 mesh was used for case $q_w = 10\,\mathrm{W \cdot m^{-2}}$ and 256×1024 mesh for $q_w = 100\,\mathrm{W \cdot m^{-2}}$. It is to be noted that the maximum local Reynolds number ($Re = u\Delta x/\nu$) obtained is lower than 10. The non-dimensional wall distance in terms of wall units (y^+) is always less than 1. The dimensionless time step (Δt) varies from 2×10^{-3} to 5×10^{-5}.

BOUNDARY CONDITIONS

The boundary conditions are $\frac{\partial \theta}{\partial x}(x = 0, z) = 1$ on the thermally active wall, and $\frac{\partial \theta}{\partial x}(x = b/H, z) = 0$ on the adiabatic wall. A non-slip boundary condition for the velocity is imposed along the walls and due to the PISO method, Neumann boundary conditions are imposed along the walls for the pressure. The imposed conditions at inlet ($z = 0$) are: $\theta = 0$; $u = \frac{\partial w}{\partial z} = 0$.

Table 1: Numerical cases with different parameters which have been investigated in the study

	Ra_H			5.89×10^9	2.95×10^{10}	4.42×10^{10}	5.89×10^{10}
	q_w ($\mathrm{W \cdot m^{-2}}$)			10	50	75	100
	grid 2D			(64×512)	(128×512)	(128×1024)	(256×1024)
BC	b (m)	i (°)	H/b	$Ra_m \cos(i)$			
GB-0	0.05	0	12.8	1.71×10^4	8.57×10^4	1.29×10^5	1.71×10^5
	0.05	45	12.8	1.21×10^4	6.06×10^4	9.09×10^4	1.21×10^5
	0.05	60	12.8	8.57×10^3	4.29×10^4	6.43×10^4	8.57×10^4
	0.05	75	12.8	4.44×10^3	2.22×10^4	3.33×10^4	4.44×10^4
LB-LB	0.06	0	10.67	4.27×10^4	2.13×10^5	3.20×10^5	4.27×10^5
	0.0985	0	6.5	5.09×10^5	2.54×10^6	3.82×10^6	5.09×10^6
	0.0985	45	6.5	3.60×10^5	1.80×10^6	2.70×10^6	–
	0.0985	60	6.5	2.54×10^5	1.27×10^6	1.91×10^6	–

At the outlet ($z = 1$): if $\vec{V}.\vec{n} < 0$, then $\theta = 0$, else $\frac{\partial \theta}{\partial x}(x,1) = 0$; $u = \frac{\partial w}{\partial z} = 0$.

The boundary condition for the pressure at the open ends of the domain requires special attention. Indeed, the induced flow in the channel results from the balance between the buoyancy forces generated by the heat transfer along the channel walls and the pressure losses between the inlet and the outlet of the channel. The mass flow rate is not known a priori, and the velocity distribution is no more known neither at the inlet nor at the outlet. Thus, in order to avoid external extended domain, we choose to imposed artificial pressure boundary conditions at the inlet of the channel, derived from Bernoulli equation, either in global or local form.

- Global Bernoulli boundary condition (GB) :

$$P(x,z) = -\frac{1}{2}\left(\int_0^1 w(x,z)dx\right)^2 = \frac{1}{2A_{in}^2}G^2 \quad (5)$$

  where G is a dimensionless mass flow rate and A_{in} is the inlet area.

- Local Bernoulli boundary condition (LB) :

$$P(x,z) = -\frac{1}{2}w(x,z)^2 \quad (6)$$

At the outlet, a free jet condition is also considered, depending on the flow direction : $P = 0$ if $V.n > 0$. Four resulting sets of boundary conditions are synthesized through notations (GB-0, GB-LB, LB-0 and LB-LB) according to Table 2. For example, the set of boundary condition GB-LB is presented (Figure 2): a Global Bernoulli condition (Eq.5) is used at the inlet, and at the outlet, a Local Bernoulli condition (Eq.6) is imposed, if $V.n < 0$, and a free jet condition if $V.n > 0$.

Table 2: Pressure boundary condition

		Inlet	
		GB	LB
Outlet	0	GB-0	LB-0
	LB	GB-LB	LB-LB

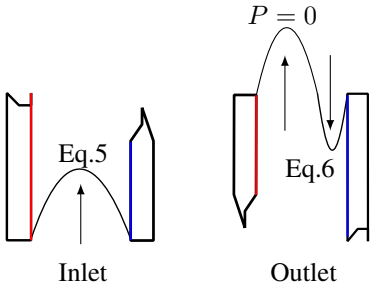

Figure 2: Example boundary condition (GB-LB)

The choice of these boundary conditions implies that the flow is not disturbed at the channel inlet and that the surrounding environment does not influence the flow within the channel. These conditions of non-interference of the surrounding environment are difficult to obtain experimentally for buoyant induced flow, and this must be kept in mind when comparing with experimental results.

RESULTS AND DISCUSSION

Boundary conditions comparison in 2D and 3D

The numerical results obtained from the CFD modeling were compared to experimental data for an aspect ratio $H/b = 10.7$ and a height-based Rayleigh number $Ra_H = 5.9 \times 10^9$ ($q_w = 10\,\mathrm{W \cdot m^{-2}}$) detailed in (Dupont et al., 2007).

The profiles of the vertical velocity normalized by the bulk velocity (w/V_b) are shown in Figures 3(a) and 3(b) at $z/H = 0.078$ and $z/H = 0.859$ respectively. Figure 3(a) shows that the penetration into the channel is preferably done by the heated side of the channel.

The inlet velocity profiles differs from the experimentation, whatever the set of boundary conditions (Figure 3(a)). The use of a uniform pressure (GB) induces an asymmetric Poiseuille type velocity profile, while a local pressure boundary condition (LB) provides an essentially flat velocity profile.

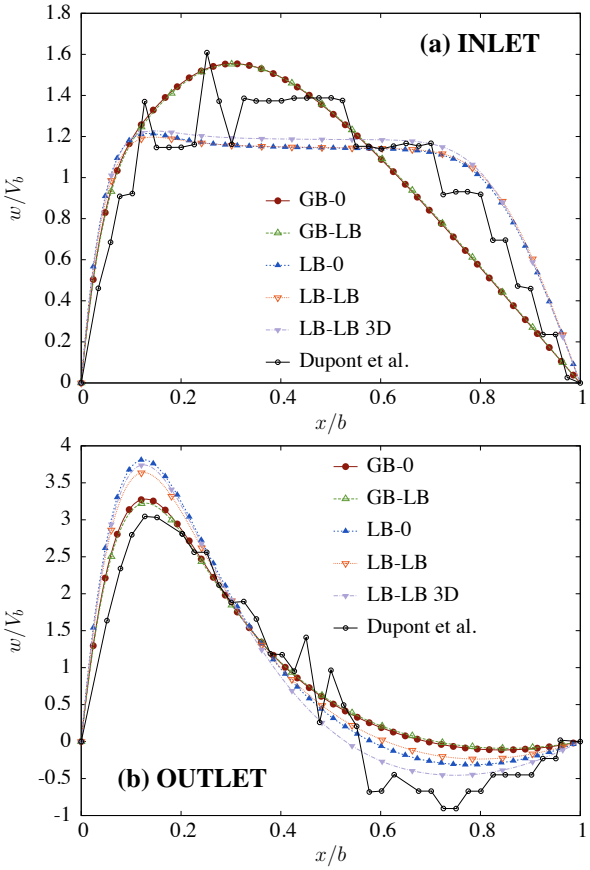

Figure 3: Vertical velocity profiles w/V_b. Comparison between numerical and experimental results for $Ra_{_H} = 5.9 \times 10^9$, $H/b = 10.7$ and $i = 0\,°$. (a) $z/H = 0.078$. (b) $z/H = 0.859$

Another difference can be observed in (Figure 3(b)), where local pressure boundary condition induces a more pronounced reverse flow than a global pressure condition along the adiabatic side of the channel at $z/H = 0.859$. Generally, we can notice than the computed vertical velocity is overestimated along the heated wall whereas the reverse flow is numerically underestimated along the cold wall.

Three-dimensional direct numerical simulation with the LB-LB boundary condition set have then been performed. Non-slip boundary conditions are applied for the velocity along the walls in the y-direction. The vertical velocity profiles displayed in the Figure 3(a) show that similar profiles are obtained at the inlet between the 2D and 3D cases. However 3D results better represent the reverse flow and slightly improves the comparison with the experimental data through the whole outlet section of the channel.

A summary of the averaged flow quantities is presented in Table 3 for direct comparison between the different cases we considered. The computed value of the bulk velocity (V_b) for the (LB-LB) set of boundary condition goes along with the experimentally observed one. Generally the Local pressure condition (LB) estimates more precisely the bulk velocity than a Global condition (GB), with a difference less than 2% with the experimental value ($V_b = 0.043\,\mathrm{m \cdot s^{-1}}$). Moreover, applying global boundary conditions at the inlet section produces larger flow rates (q_v) than applying local pressure conditions. Concerning the heat transfer at the heated wall, the Nusselt numbers at the mid-height of the channel ($\mathrm{Nu}_{1/2}$) are reported in Table 3. We observe than the different sets of boundary conditions lead to an underestimation of the energy transfer compared to the experimental one, with slightly higher values when applying Global boundary conditions.

Table 3: Summary of the flow results for $Ra_{_H} = 5.9 \times 10^9$, $H/b = 10.7$ and $i = 0\,°$

	V_b	q_v	$\mathrm{Nu}_{1/2}$
	$(\mathrm{m \cdot s^{-1}})$	$(\mathrm{m^3 \cdot s^{-1}})$	–
Dupont et al. (2007)	0.043	–	5.530
GB-0	0.047	3.113	5.337
GB-LB	0.048	3.173	5.343
LB-0	0.040	2.639	5.225
LB-LB	0.042	2.771	5.239
3D LB-LB	0.042	2.765	5.242

The experimental velocity fields obtained with a Laser Doppler Anemometry technique is represented in Figure 4. The use of this sophisticated technique has been adopted by Dupont et al. due to its low intrusiveness, its spatial resolution and its capacity to differentiate the sign of the velocity.

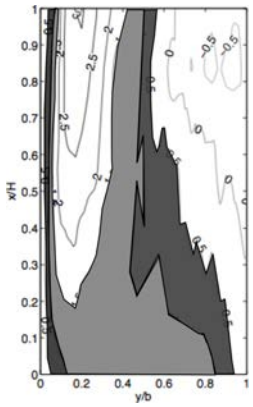

Figure 4: Experimental data. Iso-contours of w/V_b in the channel. $H/b = 10.7$ and $Ra_H = 5.9 \times 10^9$ ($Ra_m \cos(i) = 4.27 \times 10^4$, $q_w = 10\,\mathrm{W \cdot m^{-2}}$, $i = 0\,°$). The iso-contours are distributed from -0.5 to 3.0 (Samot et al., 2010)

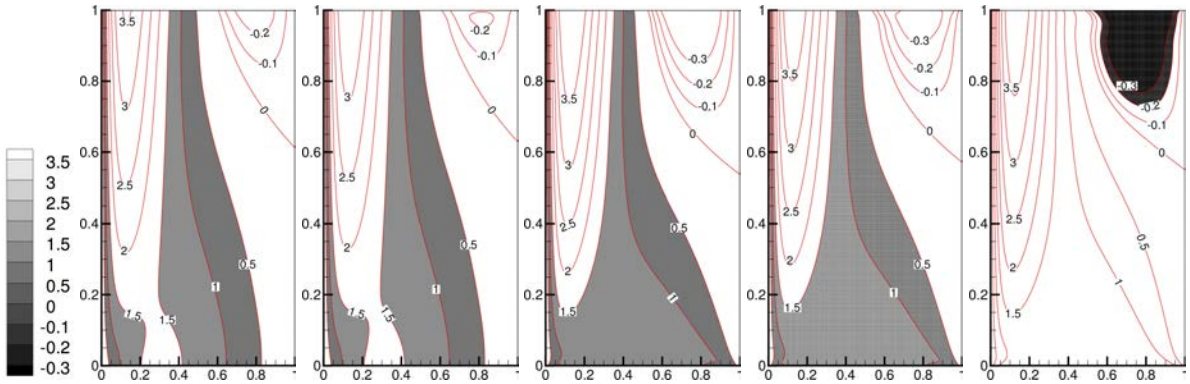

(a) GB-0 (b) GB-LB (c) LB-0 (d) LB-LB (e) 3D LB-LB

Figure 5: Iso-contours of the dimensionless w/V_b in the channel for different boundary conditions. $H/b = 10.7$ and $Ra_H = 5.9 \times 10^9$ ($Ra_m \cos(i) = 4.27 \times 10^4$, $q_w = 10\,\mathrm{W \cdot m^{-2}}$, $i = 0\,°$). The iso-contours are distributed from -0.3 to 3.5

Figure 5 shows the numerical iso-velocity fields for the four sets of boundary conditions we considered. Comparison of (Figure 5(c) and Figure 5(d)) shows than Local Boundary conditions produce a better representation of the flow in the lower section of the channel than Global Boundary conditions. The extension of the reversal flow region is also greater for LB conditions and the intensity of the reverse flow is slightly larger when this local formulation is used (Figure 5(c) and Figure 5(d)) versus (Figure 5(a) and Figure 5(b)). As already noted in Figure 3, 3D DNS (Figure 5(e)) improves the prediction of the intensity of the reversal flow.

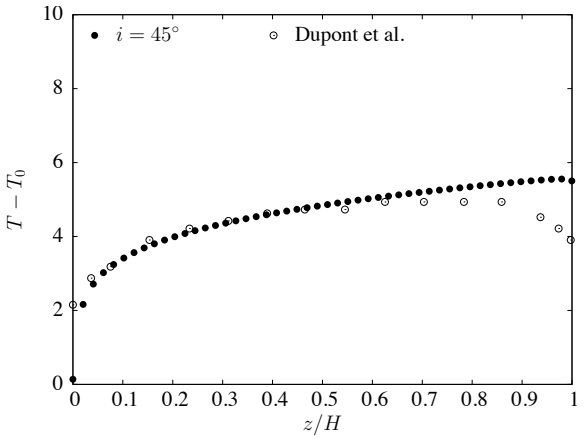

Figure 6: Wall temperature distribution along the heated wall by $Ra_H = 5.9 \times 10^9$, $H/b = 6.5$ and $i = 45\,°$

If we compare now the temperature evolution along the heated wall (Figure 6) we observe different behaviours between the numerical and the experimental distributions. In this case, the parietal temperature decreases in the upper section of the channel, whilst it continuously grows for the numerical investigation. This difference probably comes from the radiative exchanges between the surrounding walls of the test room and the channel outlet. These exchanges are not taken into account in our numerical results, but various numerical investigations (Zoubir et al., 2011; Li et al., 2011; Mittelman et al., 2009) report that the flow is extremely sensitive to radiation exchanges between the walls, and can dramatically change the flow structure as far as preventing the existence of a reversal flow.

Existence of a reversal flow

From laser tomography visualizations, (Samot et al., 2010) explored the conditions of existence of a reverse flow in their channel, and established the following conclusions (Figure 4):

- for values of the aspect ratio H/b between 9.14 and 16 and height-based Rayleigh number (Ra_H) less than 4.46×10^{10}, a permanent reversal flow exists,
- for values of aspect ratio H/b between 18.29 and 25.6 or less than 9; an intermittent reversal flow is observed,
- for values of the aspect ratio H/b greater than 25.6; reversal flow do not exist.

Considering our numerical investigation, we observe a permanent reverse flow in all of theses cases, sometimes with very weak amplitude, but always present.

Heat transfer correlations

Several authors have investigated the heat transfer inside a tilted thermosyphon, as an example (Azevedo and Sparrow, 1985; Manca and Nardini, 2001; Chungloo and Limmeechokchai, 2009; Chami and Zoughaib, 2010). In this later part of the paper, our study is compared with their results.

Table 4: Nusselt correlations

Ref	Correlations	
Webb and Hill (1989)	$\mathrm{Nu}_{1/2} = 0.58(Ra_m \cos(i))^{0.206}$	(8)
Dupont et al. (2007)	$\mathrm{Nu}_{1/2} = 0.59(Ra_m \cos(i))^{0.206}$	(9)
present study	$\mathrm{Nu}_{1/2} = 0.61(Ra_m \cos(i))^{0.199}$	(10)
	$\mathrm{Nu}_{1/2} = 0.72(Ra_m \cos(i))^{0.187}$	(11)

Figure 7 present the Nusselt number at mid-height of the cavity, $\mathrm{Nu}_{1/2}$, for various values of $Ra_m \cos(i)$ compared with the results of (Dupont et al., 2007) (Table 4, Eq.8) and with the proposed correlation of (Webb and Hill, 1989) (Table 4, Eq.9). Few differences exists between the choice of a local (LB-LB) and global pressure (GB-0) condition within the results on the mid-height Nusselt numbers. The results presented in this study are very closed to those obtained by Dupont et al. and match pretty well with Eq.8 with a relative difference less than 2% up to $Ra_m \cos(i) = 2 \times 10^5$, (see Table 4). For better accuracy, we divided the whole domain we considered in two sub domains, and we derived correlations for each of theses domains. The first correlation (Eq.10, Table 4) is valid in the range $4 \times 10^3 < Ra_m \cos(i) \leq 2 \times 10^5$ and the second correlation (Eq.11, Table 4) is valid in the range $2.5 \times 10^5 < Ra_m \cos(i) \leq 5 \times 10^6$.

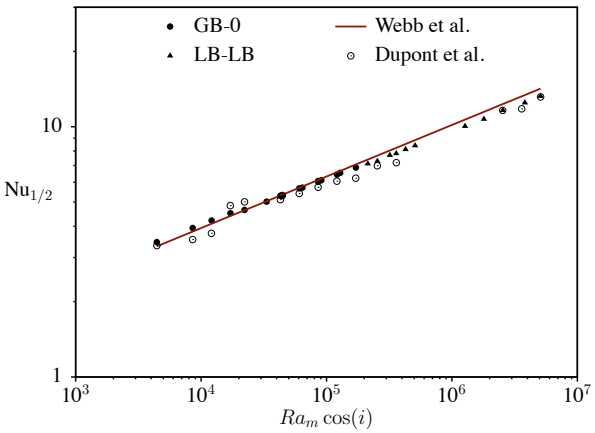

Figure 7: Average Nusselt number vs modified Rayleigh number for channel aspect ratios of 6.5, 10.67 and 12.8. Comparison between numerical and experimental data of (Webb and Hill, 1989) and (Dupont et al., 2007)

CONCLUSION

We implemented a numerical approach to study the natural convection flows in inclined open channels. The study was based on an experimental configuration set up by (Dupont et al., 2007) and the comparison with their experimental data was led. The comparison reveals a correct qualitative accord, but however, differences exist for the domain of existence of a return flow in the upper part of the channel, which brings us to consider the influence of surface radiation on the flow. In fact, surface radiative exchanges influence the flow, particularly near the inlet and outlet sections, and must be considered in this type of configuration. The first results presented in this study will thus be completed in the near future by integrating surface radiation. Comparisons with the experimental data, allowed us to highlight the importance of properly chosen boundary conditions for open geometries. We observe than local pressure boundary conditions at the inlet/outlet sections (LB-LB) improve the results when compared to global conditions (GB). Three-dimensional effects were also studied, and show negligible effects for the main upward flow but improve the prediction of the reverse flow.

ACKNOWLEDGEMENT

This work has been supported by French Research National Agency (ANR) through "Habitat intelligent et solaire photovoltaïque" program (project 4C n°ANR-08-HABISOL-019). The authors thank greatly Dr.Frédéric Dupont for furnishing experimental data from the GRER experiment.

REFERENCES

Andreozzi, A., Buonomo, B., and Manca, O. 2007. Numerical investigation on natural convection in asymmetric channel-chimney systems. In *WIT Transactions on Modelling and Simulation*, volume 46, pages 389–398.

Azevedo, L. F. A. and Sparrow, E. M. 1985. Natural convection in open-ended inclined channels. *Journal of heat transfer*, 107(4):893–901.

Bar-Cohen, A. and Rohsenow, W. 1984. Thermally optimum spacing of vertical, natural convection cooled, parallel plates. *Journal of Heat Transfer*, 106(1):116–123.

Bassiouny, R. and Korah, N. 2009. Effect of solar chimney inclination angle on space flow pattern and ventilation rate. *Energy and Buildings*, 41(2):190–196.

Campo, A., Manca, O., and Morrone, B. 1997. Inflow and outflow effects on natural convection in partially heated vertical parallel plate channels. In *American Society of Mechanical Engineers, Heat Transfer Division, (Publication) HTD*, volume 351, pages 325–335.

Chami, N. and Zoughaib, A. 2010. Modeling natural convection in a pitched thermosyphon system in building roofs and experimental validation using particle image velocimetry. *Energy and Buildings*, 42(8):1267–1274.

Chungloo, S. and Limmeechokchai, B. 2009. A field study of free convection in an inclined-roof solar chimney. *Science Asia*, 35:189–195.

Dupont, F., Soubdhan, T., Blonbou, R., Tuhault, J., Penot, F., and Soubdhans, T. 2007. Etude expérimentale de la convection naturelle en canal vertical chauffé à flux constant : Influence de l'angle d'inclinaison. In *Congrés Francais de Thermique*, page 6, Île des Embiez.

Elenbaas, W. 1942. Heat dissipation of parallel plates by free convection. *Physica*, 11(9):1–23.

Hamel, G. 1916. Spiralfömrige bewegungen zäher flüssigheiten. *Jahresbericht der Deutschen Mathematiker-Vereinigung*, 25:34–60.

Henkes, R. and Hoogendoorn, C. 1995. Comparison exercise for computations of turbulent natural convection in enclosures. *Numerical heat transfer. Part B, fundamentals*, 28(1):59–78.

Issa, R. 1986. Solution of the implicitly discretised fluid flow equations by operator-splitting. *Journal of Computational Physics*, 62(1):40–65.

Jeffery, G. 1915. The two-dimensional steady motion of a viscous fluid. *Philosophical magazine*, 29:455–465.

Le Quéré, P. 2008. On the computation of some external or partially enclosed natural convection flows. In *The 19th International Symposium on Transport Phenomena*, pages 1–8, Reykjavik, ICELAND.

Li, R., Sun, H., Chénier, E., and Lauriat, G. 2011. Effet du rayonnement surfacique sur les recirculations de convection naturelle. In *Congrès Français de Thermique*, pages 181–186, Perpignan.

Manca, O. and Nardini, S. 2001. Thermal design of uniformly heated inclined channels in natural convection with and without radiative effects,. *Heat Transfer Engineering*, 22(2):13–28.

Mittelman, G., Alshare, A., and Davidson, J. 2009. A model and heat transfer correlation for rooftop integrated photovoltaics with a passive air cooling channel. *Solar Energy*, 83(8):1150–1160.

Naylor, D., Floryan, J. M., and Tarasuk, J. D. 1991. Numerical study of developing free convection between isothermal vertical plates. *Journal of Heat Transfer*, 113(3):620–626.

Popa, C., Ospir, D., Fohanno, S., and Chereches, C. 2012. Numerical simulation of dynamical aspects of natural convection flow in a double-skin façade. *Energy and Buildings*, 50:229–233.

Samot, S., Dupont, F., and Penot, F. 2010. Mesure de température dans un écoulement renversé à la sortie d'un thermosiphon vertical chauffé à flux constant. In *Congrés Francais de Thermique*, page 6, Touquet.

Sparrow, E., Chrysler, G., and Azevedo, L. 1984. Observed flow reversals and measured-predicted nusselt numbers for natural convection in a one-sided heated vertical channel. *Journal of Heat Transfer*, 106(2):325–332.

Suárez, C., Joubert, P., Molina, J. L., and Sánchez, F. J. 2011. Heat transfer and mass flow correlations for ventilated facades. *Energy and Buildings*, 43(12):3696–3703.

Webb, B. and Hill, D. 1989. High Rayleigh number laminar natural convection in an asymmetrically heated vertical channel. *Journal of Heat Transfer*, 111(3):649–656.

Zoubir, A., Xin, S., Giroux-Julien, S., and Ménézo, C. 2011. Étude numérique des transferts thermoconvectifs dans un canal d ' air vertical à flux imposé. In *Société Française de la Thermique*, page 8, Perpignan.

NOMENCLATURE

Dimensionless terms

θ	dimensionless temperature	$[-]$
A	surface area	$[-]$
G	dimensionless flow rate	$[-]$
P	dimensionless modified pressure	$[-]$
Pr	Prandtl number (ν/κ)	$[-]$
Ra_H	height-based Rayleigh number $\left(Ra_m \left(\frac{H}{b}\right)^5\right)$	$[-]$
Ra_m	modified Rayleigh number $\left(\frac{g\beta q_w b^4}{\lambda\nu^2}\frac{b}{H}Pr\right)$	$[-]$
Re	Reynolds number $\left(\frac{Vb}{\nu}\right)$	$[-]$
t	dimensionless time	$[-]$
u, w	dimensionless fluid velocities	$[-]$
V_b	bulk velocity based on the on w	$[-]$
x, y, z	dimensionless cartesian coordinates	$[-]$

Greek letters

β	volumetric coefficient of thermal expansion	$[1/K]$
δ	Kronecker delta	
κ	thermal diffusity	$[\mathrm{m}^2 \cdot \mathrm{s}^{-1}]$
λ	thermal conductivity	$[\mathrm{W} \cdot \mathrm{m}^{-1} \cdot \mathrm{K}^{-1}]$
ν	kinematic viscosity	$[\mathrm{m}^2 \cdot \mathrm{s}^{-1}]$

Latin letters

ΔT	temperature difference ($q_w b/\lambda$)	[K]
$\vec{V}$	velocity vector	$[\mathrm{m}\cdot\mathrm{s}^{-1}]$
b	characteristic width	[m]
g	gravitational acceleration	$[9.81\,\mathrm{m}\cdot\mathrm{s}^{-2}]$
H	channel height	[m]
i	inclination angle	[°]
q_w	heat wall flux	$[\mathrm{W}\cdot\mathrm{m}^{-2}]$
V_{ref}	reference velocity $\left(\frac{\kappa}{H} Ra_H^{1/2}\right)$	$[\mathrm{m}\cdot\mathrm{s}^{-1}]$

Abreviations

0	reference
BC	boundary condition
GB	global Bernoulli condition
LB	local Bernoulli condition